

Molecular-Scale Hydrophilicity Induced by Solute: Molecular-thick Charged Pancakes of Aqueous Salt Solution on Hydrophobic Carbon-based Surfaces

Guosheng Shi^{1†}, Yue Shen^{1,2†}, Jian Liu^{1,3}, Chunlei Wang¹, Ying Wang¹, Bo Song¹, Jun Hu¹, and Haiping Fang^{1*}

¹*Division of Interfacial Water and Key Laboratory of Interfacial Physics and Technology, Shanghai Institute of Applied Physics, Chinese Academy of Sciences, Shanghai 201800, China*

²*Salt Lake Resources and Chemistry Laboratory, Qinghai Institute of Salt Lakes, Chinese Academy of Sciences, Xining 810008, China*

³*University of Chinese Academy of Sciences, Beijing, 100049, China*

†These authors contributed equally to this work.

*Email: fanghaiping@sinap.ac.cn

ABSTRACT: We show the direct observation of the molecular-thick aqueous salt solution pancakes on the hydrophobic graphite surface under ambient conditions at room temperature by using atomic force microscopy imaging. This indicates the unexpected molecular-scale hydrophilicity of the salt solution on the graphite surfaces, which is different from their macroscopic wetting property — a droplet still stands on the graphite surface. Interestingly, the pancakes spontaneously display high positively charged behavior. Theoretical studies showed that the formation of such positively-charged pancakes was attributed to the cation- π interactions between Na^+ in the aqueous solutions and aromatic rings on the graphite surfaces, promoting the adsorption of water molecules together with cations onto the graphite surfaces, i.e., Na^+ as a medium one side adsorbed graphite surface by cation- π interactions, at same times the other side adsorbed water molecules by hydration interaction at molecular scale. These findings suggest that the actual interactions regarding the carbon-based graphitic surface including graphene, carbon nanotube, biochar may be significantly different from the existing theory and provides new insight to the control of surface wettability, interactions and related physical, chemical and biological processes.

INTRODUCTION

Hydrophilic/hydrophobic interactions are among the most important driving forces in various physical phenomena,¹⁻²⁵ such as wetting/dewetting,¹⁻⁵ protein folding and its

native structure formation,⁶⁻⁹ drug/molecular delivery,^{10,11} water purification/desalination,^{12,13} molecular recognition¹⁴ and nanoparticle assembly/self-assembly in aqueous solution.^{15,16} Conventionally the wetting property of a surface is determined from the macroscopic behavior of water, i.e., contact angles of water droplets on the surface, which is widely used to analyze the interactions of the solid surface with other materials and dynamics property at the interface, however, these interactions and dynamics property in fact are dominated by the behavior of water molecules of molecular-thickness on the surface. In recent years, molecular-thickness aqueous films have been observed on various hydrophilic surfaces¹⁻⁴ and between two surfaces¹⁷. On the contrast, on the typical hydrophobic carbon-based surfaces, such as the graphene/graphite surfaces, water films are known to only adsorb below an extremely low temperature.²

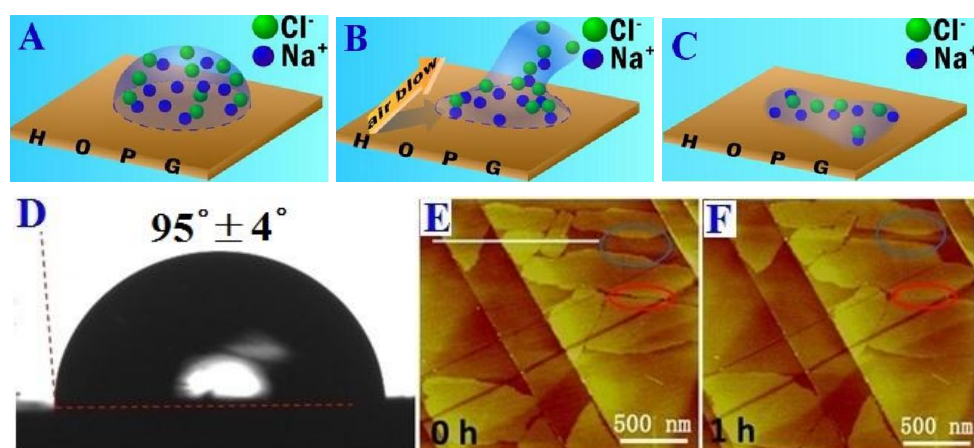
Carbon-based surfaces widely exist in both nanoscale and macroscopic materials,²⁶⁻³⁴ and most of them contain a graphitic surface (composed of many aromatic rings which is a hexagonal carbon rings with rich π electrons), such as graphite, graphene,^{27,28} carbon nanotube,^{29,30} fullerene,³¹ biochar^{32,33} and activated carbon³⁴. Moreover, graphitic surfaces with rich aromatic rings also widely exist in biomolecules and organic molecules,³⁵ humus in the soil,³⁶ and polycyclic aromatic hydrocarbons (PAHs) in air pollutants³⁷. It is well-recognized that most of these aromatic rings rich graphitic surfaces are hydrophobic and their wetting properties are similar to those of graphite. However, some phenomena that only exist on the hydrophilic surfaces have been recently observed on these graphitic carbon-based surfaces.^{32-34,38-40} For examples, it has been found that biochar significantly increases water retention in a sandy soil whereas biochar is well-recognized as hydrophobic.^{32,33} The wetting and charge characteristics of graphene and graphitic surfaces are significantly impacted by its deposited substrates^{38,39} and adsorbed airborne/atmospheric contaminants^{40,41}. As stated above, the water wetting properties on graphitic surfaces are complicated and are still far from being fully understood.

Interface characteristics between the graphitic surface and their surroundings, especially for the water and ions environment, are believed to be the heart of the property and application for these carbon-based nanomaterials.²⁷⁻⁴⁵ We note that although the aromatic rings only have weak interactions with water, they have strong interactions with cations, which named as cation- π interaction.⁴⁶ Therefore, we expect that the behavior of the water close to the aromatic rings will be greatly changed when there are cations involved.^{47,48} Unfortunately, in the wetting property of surfaces, the role of the cation- π interactions has still been ignored in spite of its importance in the control of the structure and function of microscale and nanoscale materials, macromolecules and proteins have been extensively exploited.^{35,49-52}

In this paper, we show the direct observation of the molecular-scale aqueous salt solution pancakes on the typical hydrophobic carbon-based surfaces, the graphite surfaces, under ambient conditions at room temperature. We note that the molecular-thick liquid films have been observed experimentally on the hydrophilic mica surface^{1,2} and on the graphitic surfaces (including graphene) water films are known to only adsorb on the graphitic surfaces below ~ 150 K.² Thus, our observation indicates the unexpected molecular-scale hydrophilicity to the salt solution on those hydrophobic surfaces since macroscopic large salt solution droplets can still be formed on the same surfaces. The cation- π interactions together with the different properties of graphitic surface and Na^+ ions distribution between the molecular and macroscopic scale result in the wetting property inconsistency between molecular (hydrophilicity) and macroscopic (hydrophobicity) scale. Moreover, the pancakes spontaneously display high positively charged behavior. The findings are expected to raise extensive applications such as the interactions of biomolecules, treatment of heavy metal ions pollution in the soil or water, and ions storage and detection.

RESULTS AND DISCUSSION

We deposited a drop of NaCl solution or pure water of mm dimensions onto a freshly-cleaved highly oriented pyrolytic graphite (HOPG) sheet, and both of them form large macroscopic droplets on the graphite surface. The static contact angles (SCAs) of NaCl solution and pure water on HOPG surface are measured, with the average values of $95^\circ \pm 4^\circ$ for NaCl solution (see Fig. 1D) and $93^\circ \pm 2^\circ$ for the pure water (see Fig. S1D). Then an air blow was used to remove the aqueous droplets (for NaCl solution, schematic drawings, Fig 1(A-C); for pure water, see supporting materials). The systems were at room temperature and $\sim 40\%$ RH.



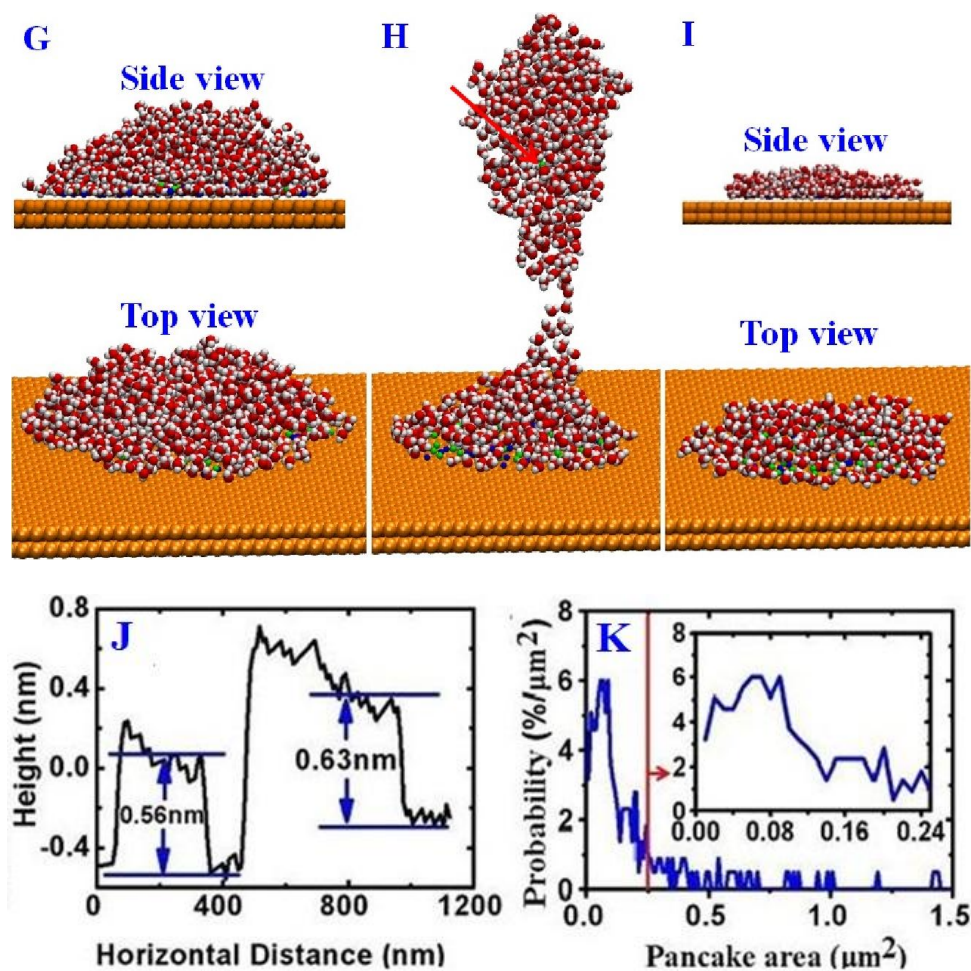


Figure 1. (A-C) Schematic drawings of the sample preparation in experiment. (A) Deposition of a drop of NaCl solution onto a freshly-cleaved highly oriented pyrolytic graphite (HOPG) sheet. (B) Some of solution removed by an air blow. (C) Resulted aqueous pancake (note that figure is not drawn to scale). (D) A macroscopic droplet of aqueous salt solution on the HOPG surface. Average static contact angle (SCA) value of NaCl solution on the HOPG surface is $95^\circ \pm 4^\circ$, which is very close to the average SCA value of $93^\circ \pm 2^\circ$ of pure water. (E,F) AFM images of the highly oriented pyrolytic graphite (HOPG) surface at RH of about 40%. (E) AFM image of graphite surface after an air blow was used to remove the aqueous droplet: the red ring indicates the boundary of a single pancake and follows its changes in shape over time. The blue ring indicates the formation of a bulge at the edge of the pancake. (F) One hour after treatment with the salt solution, as shown in (E). Pancake gradually enlarged and a visible bulge appeared at the edge in blue ring. (G-I) Snapshots from molecular dynamics simulations. (G) A NaCl solution droplet on a graphite surface. (H) A snapshot of the system when the salt solution were driven upper right, i.e., an acceleration of 0.10 nm/ps^2 was applied to all the water and ions along the midline between the x and z directions to study the impact of the blowing air on the system during experimental preparation. (I) NaCl solution pancake onto a graphite surface after the water molecules were driven upper right for 2 ns. In G, H and I, the orange structures depict the graphite sheets; water molecules, sodium and chlorine ions are shown with oxygen in red, hydrogen in white, sodium in

blue and chlorine in green. (J) A height profile corresponding to the white line in (E) showing the layer is about 0.6 nm high relative to the substrate. (K) The distribution probability of the micro pancake areas. The upper right corner small figure denotes an enlargement of the left region marked by the red line.

Usually, if the salt concentration was high, many salt particles and aggregates could be seen left on the graphite and if the concentration was too low, the surface would be clean and nothing could be observed. However, under the salt concentration of ~ 20 mM, sometimes we could observe many thin films of the salt solution (we termed them as pancakes) on the HOPG surface by tapping mode atomic force microscopy (AFM) imaging in most of the cases as shown in Fig. 1(E), at ~ 10 min after being treated by the salt solution (see detail in supporting information). In most cases, the apparent heights of those pancakes are about 0.6 nm (Fig. 1(J)), and in some cases, the apparent heights are about 0.3 nm. The lateral length scale of those pancakes spans from a few hundreds of nanometers to several micrometers, which is about 3-4 orders of magnitude larger than their heights. In one experiment, we determined the probability distribution of the areas of 217 pancakes we observed (Fig. 1 (K)). From this distribution, we computed the average area as $0.20 \mu\text{m}^2$. We also found that the pancakes existed at different humidities of 30% - 70% RH and no pancakes appeared on the surfaces treated only by pure water (see supporting material).

The pancakes appeared movable across the graphite surfaces over time. The AFM images of the surfaces acquired after 1 hour are quite different from those acquired after 10 min after being treated by the salt solution (Fig. 1(F) vs. Fig. 1 (E)). For example, the pancake gradually enlarged and a visible bulge appeared at the edge (Fig. 1(F)). The boundary distance between the pancake and nearby pancakes decreased, and over time the pancake gradually coalesced with surrounding pancakes. These movable behaviors of the pancakes enlarging and coalescing result in the lower charge distribution and surface energy (see details in Supporting Information).

We have also used AFM of **non-contact** mode vibrating scanning polarization force microscopy (VSPFM) to image the HOPG surface treated by the salt solution to minimize the effect of the AFM tips. As shown in Fig. S3 in the supporting material, movable solution pancakes can also be clearly seen. The movable behavior of the pancakes has been further demonstrated by the repair of a partially damaged pancake and the behavior of a thoroughly removed pancake shown in supporting material. These observations suggest that the pancakes are composed of liquid.

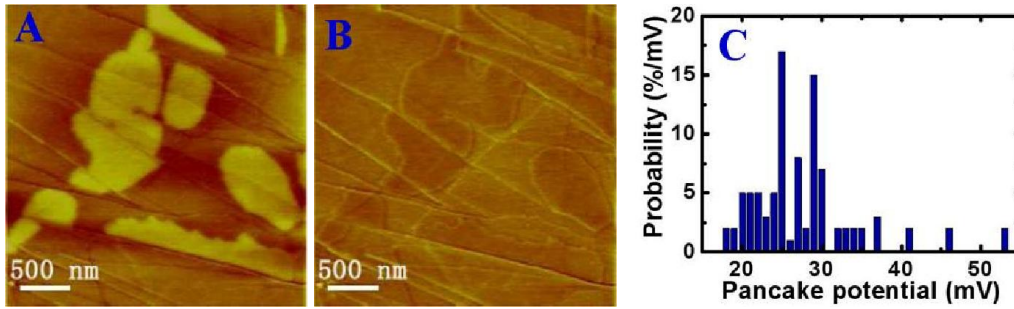


Figure 2. Electrical properties of the NaCl solution pancake. A typical EFM image with the 3V tip voltage (A) and -3V tip voltage (B). (C) The distribution probability of the electric potentials of 60 pancakes.

Remarkably, the salt solution pancakes showed non-charge-neutral behavior. The electrostatic force microscopy (EFM) image obtained with a +3 V tip voltage (Fig. 2(A)) showed clear bright pancakes, and these pancakes darkened when the voltage was -3V (Fig. 2(B)). By using Kelvin probe force microscopy images (KPFM), we obtained the values of the potentials on the pancakes relative to the substrate. We measured the probability distribution of the electric potentials of 60 pancakes and determined the average pancake potential to be ~ 27 mV (Fig. 2, C).

The observed liquid pancakes on HOPG are out of the conventional expectation since the HOPG surface is hydrophobic and the salt solution would like to form droplets (Fig. 1D). During the NaCl droplets drying process, the left salt should form particles or aggregates of small particles on HOPG at 40% RH, which is far below the deliquescence humidity of NaCl (around 75% at the room temperature⁵³). Clearly, this fact indicates that the hydrophobic graphite surfaces showed “apparent” and strong molecular-scale hydrophilicity with respect to the salt solution under ambient conditions.

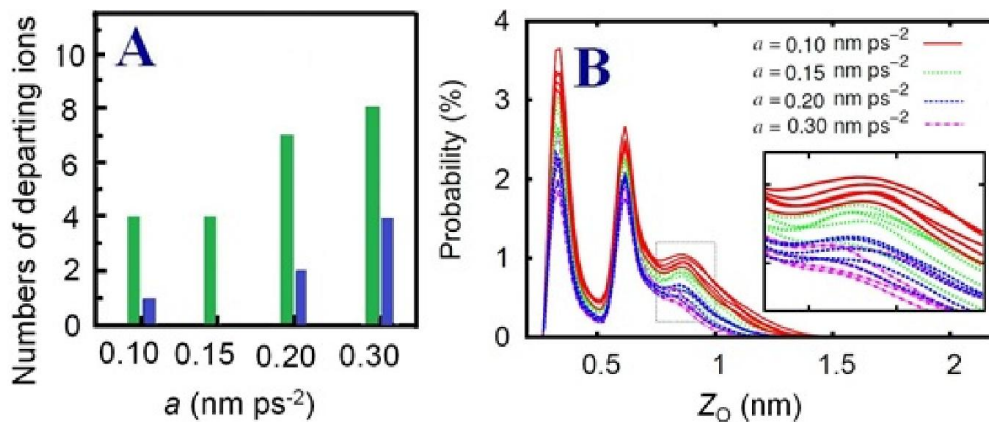


Figure 3. (A) Total numbers of Cl⁻ (green ribbons) and Na⁺ (blue ribbons) departed with the solution disconnected from other solution on the graphite surface for five parallel samples at each

acceleration value a . (B) Distribution probability of the oxygen atoms along the z direction in the resulting aqueous pancakes.

The physics mechanism for those unexpected charged solution pancakes are the cation- π interactions. The graphite surface adsorbed the ions; the water molecules were then adsorbed onto the surface with the help of the ions.⁴⁷ To further demonstrate the hydrophobic/hydrophilic transition due to the Na^+ adsorption onto graphite, we performed molecular dynamics (MD) simulations with a cation- π interaction modification⁴⁸ of the NaCl solution on graphite. We mimic these behaviors by applying additional accelerations a along the line between the x and z directions on a NaCl drop solution (including 810 water molecules and 45 sodium and chloride ions) on the graphite surface. For each system, MD simulations were performed for five parallel samples with different initial configurations, each for 2 ns. As the typical case shown in Fig. 1(G-I) where $a = 0.1 \text{ nm/ps}^2$, at $t = 0.96 \text{ ns}$, some of the solutions moved upper and became to disconnect with the other solutions (Fig. 1H) (see detail in the movie in Supporting Information). Interestingly, we found that there was a Cl^- in the part departing the surface. This result in the solution pancake left on the solid surface (see Fig. 1I) has a positive charge since there is more Na^+ . The similar variation of this charge neutrality behavior is also been observed by Martinez-Martin D. et al.⁴¹ on the graphitic surfaces for the adsorption of atmospheric contaminants, such as a polycyclic aromatic hydrocarbon (PAH) and its isomers.

Figure 3A shows that the total numbers of Cl^- and Na^+ departed with the solution disconnected from other solution on the graphite surface in different acceleration values. It is clear that there are less Na^+ than Cl^- departed from the surface, and generally, the larger acceleration, the more numbers of Na^+ and Cl^- departed from the surface. It is clear that this positive charge behavior of the pancake on the graphite surface results from the much weaker interactions between Cl^- and the graphite surface, comparing to Na^+ and the graphite surface (the hydrated Cl^- - π interaction is much smaller (-1.8 kcal/mol), which is only about 1/10 of the hydrated Na^+ - π interaction (-16.4 kcal/mol)⁴⁸).

In order to study the behavior of the solutions remained on the graphite surface, we further performed MD simulations on the remained NaCl solution for 4 ns after the blow off the disconnection solution. From the distribution probability of oxygen atoms along the z direction shown in Fig. 3B for each simulation, we can see that there are three peaks at $Z_O = \sim 0.32$, ~ 0.63 and $\sim 0.86 \text{ nm}$, respectively. The fore two peaks are consistent with the experimental observation of ~ 0.3 and $\sim 0.6 \text{ nm}$ height of the pancake structures. As a increases, the peak at $Z_O = \sim 0.86 \text{ nm}$ becomes low and even disappears. There are only 3, and 2 simulations show clear peaks at $a = 0.2$ and 0.3 nm/ps^2 . Thus, the heights of the resulted pancakes depend on the strength of the

accelerations a . We note that the existence of the charged pancakes is robust which can be clearly seen at all of four accelerations values ($a = 0.10, 0.15, 0.20$ and 0.30 nm/ps²) in our simulations. This further demonstrates the consistence between the MD simulations and the experimental observations.

We also further analyze that the main reason of the wetting property inconsistency between molecular and macroscopic scale. The flat graphite surface on the macroscopic scale is made up by a large number of graphene flakes stacking on molecular scale. The macroscopic flat graphite surface are actually formed by a large number of molecular level graphene layers, and there are a lot of steps between the layers (See Fig. 1(E,F) and Fig. 2(A,B)). Theoretical calculations based on quantum mechanics (DFT) method (see details in Supporting Information) show that the Na⁺ ions may easily diffuse on the graphene flakes (only ~ 3 kcal/mol barrier energies, Fig. S4B), while it is very difficult across the steps between layers (above 100 kcal/mol barrier energies, Fig. S4B). Thus, Na⁺ ions bind at the aromatic rings on the graphite surface retaining their hydration water molecules, resulting in molecular-thick pancakes of aqueous salt solution forming on the molecular level graphene layers (See Fig. 1(E,F)), but the salt solution drop will still remain because there are a large amount of molecular scale layer steps hindering the diffusion of Na⁺ ions on the macroscopic surface.

Moreover, the existence of a large amount of hydrophobic steps will significantly decrease the surface energy of graphite surface (Fig. S5), which cause the macroscopic graphite surface to be more hydrophobic than the molecular scale graphene flakes (see details in Supporting Information). The distribution of Na⁺ ions in the salt solution on molecular scale⁴⁸ is much easier to close the solid surface than it on macroscopic scale, which also impact on the wetting property of different (macroscopic and molecular) scale. In a word, the different properties of graphitic surface and Na⁺ ions distribution between the molecular and macroscopic scale result in the wetting property inconsistency between molecular (hydrophilicity) and macroscopic (hydrophobicity) scale.

CONCLUSION

We conclude that, counter to intuition, on the hydrophobic surfaces, molecular-thick films of aqueous salt solution can stably exist on the hydrophobic carbon-based surface under ambient conditions at room temperature, combining with the experimental and theoretical results, showing the unexpected molecular-scale hydrophilicity on the hydrophobic surfaces. The cation- π interactions together with the different properties of graphitic surface and Na⁺ ions distribution between the molecular and macroscopic scale result in the wetting property inconsistency between

molecular (hydrophilicity) and macroscopic (hydrophobicity) scale. Interestingly, the pancakes spontaneously display positively charged behavior. Considering that the key ingredients for the existence of the molecular-scale pancakes, the aromatic rings, are commonly found in biomolecules, the findings may improve the understanding of the actual interactions of biomolecules. The mechanism underlying should be helpful to the understanding and controlling of the functional characteristics of the carbon-based materials for various applications such as drug delivery, water purification based on carbon nanotubes, ion filtration of graphene pores, hydrogen storage of graphene/graphite, and other applications of carbon-based nano-materials.

MATERIALS AND METHODS

Experimental Section:

Materials. NaCl (crystal purity 99.99%) was purchased from Sinopharm Chemical Reagent Co. Ltd., and was dissolved in ELGA lab water to a final concentration of 20 mM. The highly oriented pyrolytic graphite (HOPG) was provided by Molecular Devices and Tools for Nano Technology Co. Zelenograd, Moscow, Russia. The electric conductive adhesive (DAD-40) was purchased from Shanghai Research Institute of Synthetic Resins.

Sample Preparation. The HOPG fragment was fixed to the sample holder with electric conductive adhesive with the working side up, and was freshly cleaved using double-faced adhesive tape. The NaCl sample was prepared according to a process previously reported for the observation of liquid nanodroplets of KOH by scanning polarization force microscopy⁵⁴ on graphite. Briefly, a drop (~20 μ l) of NaCl solution (20 mM) was deposited on the HOPG substrate followed by drying of the droplet with stream of air at room temperature and 40~60% RH. A sample chamber (SDH-01N, Shanghai Jianheng Instrument Co.) was used in which the RH and temperature were controlled with an accuracy of 5% and 0.1 °C, respectively. The as-prepared sample was placed in this chamber for a given amount of time.

Atomic Force Microscope (AFM) Imaging. The experiments were performed on a commercial AFM (Nanoscope IIIa, Veeco/Digital Instruments, Santa Barbara, CA) equipped with a J scanner (100 μ m \times 100 μ m) and E scanner (15 μ m \times 15 μ m). The Silicon etched probes (NSC18/Ti-Pt, MikroMasch Co., length: 230 μ m, width: 40 μ m, thickness: 3 μ m, nominated spring constant: 3.5 N/m, resonant frequency: 60-90 kHz) were used in other experiments. The Ti-Pt coating consists of a 10-nm Pt layer on a 20-nm Ti sublayer, which increases adhesion and electromigration firmness of Pt. The Ti-Pt coating is formed on both tip and reflective side of the cantilever. Resulting tip

radius with the coating is 40 nm. The morphological features of the AFM images, that is, height and width, were analyzed using the AFM-accessory software (ver. 7.30). All AFM images were adequately flattened using the software to correct the distortion at a micrometer scale, but no other digital operation was carried out. All AFM data were obtained at room temperature, whereas relative humidity was measured by a hygrometer with an accuracy of 5% (SDH-01N, Shanghai Jianheng Instrument Co.).

SCA Measurement. The SCA measurement is on an Attension Theta system (KSV Instruments Ltd., Finland). The volume of each droplet of NaCl solution and pure water is ~5 μl and each droplet is carefully touched to the sample surface. A digital camera is used to take images of all droplets, and the values of SCA are automatically computed by the supplied calculation software. Each HOPG sample is measured at three different points and the average value was reported.

Computational Methods. The cation- π interactions between Na^+ and the graphite surface are represented by a model potential.⁴⁸

$$V = \varepsilon \left(\left(\frac{z_m}{z} \right)^8 - 2 \left(\frac{z_m}{z} \right)^4 \right) \quad (1)$$

where the parameters ε and z_m are the adsorption energy and balance position distance (the vertical dimension between the Na^+ and the surface) of Na^+ with the graphite surface and z is the distance of the vertical dimension between the Na^+ and the surface, which are the main potential parameters describing the cation- π interaction. The values of them are $z_m = 3.8 \text{ \AA}$ and $\varepsilon = \varepsilon_0 = -16.4 \text{ kcal/mol}$, respectively.⁴⁸ Molecular dynamics simulations are carried out using the program NAMD2/VMD1.9 packages,⁵⁵ with the CHARMM force field,⁵⁶ at time steps of 2 fs with the O-H bonds and C atoms held fixed (see detail in Supporting Information).

REFERENCES

- [1]Hu, J., Xiao, X. D., Ogletree, D. F. & Salmeron, M. Imaging the condensation and evaporation of molecularly thin films of water with nanometer resolution. *Science* **268**, 267-269 (1995).
- [2]Xu, K., Cao, P. & Heath, J. R. Graphene visualizes the first water adlayers on mica at ambient conditions. *Science* **329**, 1188-1191 (2010).
- [3]Bonn, D., Eggers, J., Indekeu, J., Meunier, J. & Rolley, E. Wetting and spreading. *Rev. Mod. Phys.* **81**, 739-805 (2009).
- [4]Feibelman, P. J. The first wetting layer on a solid. *Phys. Today* **63**, 34-39 (2010).
- [5]Cicero, G., Calzolari, A., Corni, S. & Catellani, A. Anomalous wetting layer at the Au(111) surface. *J. Phys. Chem. Lett.* **2**, 2582-2586 (2011).
- [6]Shakhnovich, E. Protein folding thermodynamics and dynamics: where physics, chemistry, and biology meet. *Chem. Rev.* **106**, 1559-1588 (2006).
- [7]Berne, B. J., Weeks, J. D. & Zhou, R. H. Dewetting and hydrophobic interaction in physical and biological systems. *Annu. Rev. Phys. Chem.* **60**, 85-103 (2009).
- [8]Wu, Z., Cui, Q. & Yethiraj, A. Driving force for the association of hydrophobic peptides: The importance of electrostatic interactions in coarse-grained water models. *J. Phys. Chem. Lett.* **2**, 1794-1798 (2011).
- [9]Bier, D. et al. Molecular tweezers modulate 14-3-3 protein–protein interactions. *Nat. Chem.* **5**, 234-239 (2013).
- [10]Kráľ, P. & Wang, B. Material drag phenomena in nanotubes. *Chem. Rev.* **113**, 3372-3390 (2013).
- [11]Mulvery, J. J. et al. Self-assembly of carbon nanotubes and antibodies on tumours for targeted amplified delivery. *Nat. Nanotech.* **8**, 763-771 (2013).
- [12]Majumder, M., Chopra, N., Andrews, R. & Hinds, B. J. Nanoscale hydrodynamics: Enhanced flow in carbon nanotubes. *Nature* **438**, 44-44 (2005).
- [13]Powell, M R., Cleary, L., Davenport, M., Shea, K. J. & Siwy, Z. S. Electric-field-induced wetting and dewetting in single hydrophobic nanopores. *Nat. Nanotech.* **6**, 798-802 (2011).
- [14]Contreras, F.-X. et al. Molecular recognition of a single sphingolipid species by a protein's transmembrane domain. *Nature* **481**, 525-529 (2012).
- [15]Chandler, D. Interfaces and the driving force of hydrophobic assembly. *Nature* **437**, 640 (2005).
- [16]Law, A. D., Auriol, M., Smith, D., Horozov, T. S. & Buzza, D. M. A. Self-assembly of two-dimensional colloidal clusters by tuning the hydrophobicity, composition, and packing geometry. *Phys. Rev. Lett.* **110**, 138301 (2013).
- [17]Baram, M., Chatain, D. & Kaplan, W. D. Nanometer-thick equilibrium films: the interface between thermodynamics and atomistics. *Science* **332**, 206 (2011).
- [18]Coridan, R. H. et al. *Phys. Rev. Lett.* **103**, 237402 (2006).

- [19] Wang, S. et al. Enthalpy-driven three-state switching of a superhydrophilic/superhydrophobic surface. *Angew. Chem. Int. Edit.* **46**, 3915-3917 (2007).
- [20] Zhu, C., Li, H., Huang, Y., Zeng, X. C. & Meng S. Microscopic insight into surface wetting: Relations between interfacial water structure and the underlying lattice constant. *Phys. Rev. Lett.* **110**, 126101 (2013).
- [21] Wang, C. et al. Stable liquid water droplet on water monolayer formed at room temperature on ionic model substrates. *Phys. Rev. Lett.* **103**, 137801 (2009).
- [22] Bai, J. & Zeng, X. C. Polymorphism and polyamorphism in bilayer water confined to slit nanopore under high pressure. *Proc. Natl. Acad. Sci. USA* **109**, 21240-21245 (2012).
- [23] Liu, J., Wang, C., Guo, P., Shi, G. & Fang, H. Linear relationship between water wetting behavior and microscopic interactions of super-hydrophilic surfaces. *J. Chem. Phys.* **139**, 234703 (2013).
- [24] Tu, Y. et al. Destructive extraction of phospholipids from Escherichia colimembranes by graphene nanosheets. *Nat. Nanotechnol.* **8**, 594-601 (2013).
- [25] Li, H. & Zeng X. C. Two dimensional epitaxial water adlayer on mica with graphene coating: An *ab initio* molecular dynamics study. *J. Chem. Theory. Comput.* **8**, 3034-3043 (2012).
- [26] Gao, Y., Shao, N., Zhou, R., Zhang, G. & Zeng, X. C. [CTi72+]: Heptacoordinate carbon motif? *J. Phys. Chem. Lett.* **3**, 2264-2268 (2012).
- [27] Chen, D., Feng, H., & Li, J. Graphene oxide: Preparation, functionalization, and electrochemical applications. *Chem. Rev.* **112**, 6027-6053 (2012).
- [28] Grongakilas, V. et al. Functionalization of graphene: Covalent and non-covalent approaches, derivatives and applications. *Chem. Rev.* **112**, 6156-6214 (2012).
- [29] Hu, L., Hecht, D. S. & Grüner, G. Carbon nanotube thin films: Fabrication, properties, and applications. *Chem. Rev.* **110**, 5790-5844 (2010).
- [30] Dillon, A. C. Carbon nanotubes for photoconversion and electrical energy storage. *Chem. Rev.* **110**, 6856-6872 (2010).
- [31] Thilgen, C. & Diederich, F. Structural aspects of fullerene chemistry – A journey through fullerene chirality. *Chem. Rev.* **106**, 5049-5135 (2006).
- [32] Manyà, J. J. Pyrolysis for biochar purposes: A review to establish current knowledge gaps and research needs. *Environ. Sci. Technol.* **46**, 7939-7954 (2012).
- [33] Novak, J. M. et al. Characterization of designer biochar produced at different temperatures and their effects on a loamy sand. *Ann. Environ., Sci.* **3**, 195-206 (2009).
- [34] Mehta, B. A., Nelson, E. J., Webb, S. M. & Holt, J. K. The interaction of bromide ions with graphitic materials. *Adv. Mater.* **21**, 102-106 (2009).
- [35] Mahadevi, A. S. & Sastry, G. N. Cation- π interaction: Its role and relevance in chemistry, biology, and material science. *Chem. Rev.* **113**, 2100–2138 (2013).

- [36] Kogut, B. M. Assessment of the Humus Content in Arable Soils of Russia. *Eur. Soil Sci.* **35**, 843-851 (2012).
- [37] Hitzel, A., Pöhlmann, M., Schwägele, F., Speer, K. & Jira, W. Polycyclic Aromatic Hydrocarbons (PAH) and Phenolic Substances in Meat Products Smoked with Different Types of Wood and Smoking Spices. *Food Chem.* **139**, 955-962 (2013).
- [38] Rafiee, J. F. et al. Wetting transparency of graphene. *Nat. Mater.* **11**, 217-222 (2012).
- [39] Shih, C. et al. Breakdown in the wetting transparency of graphene. *Phys. Rev. Lett.* **109**, 176101 (2012).
- [40] Li, Z. et al. Effect of airborne contaminants on the wettability of supported graphene and graphite. *Nat. Mater.* **12**, 925-931 (2013).
- [41] Martinez-Martin, D. et al. Atmospheric contaminants on graphitic surfaces. *Carbon* **61**, 33-39 (2013).
- [42] Shi, G., Yang, J., Ding, Y. & Fang, H. Orbital effect-induced anomalous anion- π interactions between electron-rich aromatic hydrocarbons and fluoride. *ChemPhysChem* **15**, 2588-2594 (2014).
- [43] Shi, G., Ding, Y. & Fang, H. Unexpectedly strong anion- π interactions on the graphene flakes. *J. Comput. Chem.* **33**, 1328-1337 (2012).
- [44] Yang, J., Shi, G., Tu, Y. & Fang, H. High correlation between oxidation loci on graphene oxide. *Angew. Chem. Int. Edit.*, doi: 10.1002/ange.201404144 (2014).
- [45] Patra, N., Esan, D. A. & Král, P. Dynamics of ion binding to graphene nanostructures. *J. Phys. Chem. C* **117**, 10750-10754 (2013).
- [46] Sunner, J., Nishizawa, K. & Kebarle, P. Ion-solvent molecule interactions in the gas phase. The potassium ion and benzene. *J. Phys. Chem.* **85**, 1814-1820 (1981).
- [47] Shi, G., Wang, Z., Zhao, J., Hu, J. & Fang, H. Adsorption of sodium ions and hydrated sodium ions on the hydrophobic graphite surface via cation- π interactions. *Chin. Phys. B* **20**, 068101 (2011).
- [48] Shi, G. et al. Ion enrichment on the hydrophobic carbon-based surface in aqueous salt solutions due to cation- π interactions. *Sci. Rep.* **3**, 3436 (2013).
- [49] Dougherty, D. A. The cation- π interaction. *Acc. Chem. Res.* **46**, 885-893 (2013).
- [50] Daze, K. D. & Hof, F. The cation- π interaction at protein-protein interaction interfaces: developing and learning from synthetic mimics of proteins that bind methylated lysines. *Acc. Chem. Res.* **46**, 937-945 (2013).
- [51] Duan, M. et al. Cation \otimes 3 π : cooperative interaction of a cation and three benzenes with an anomalous order in binding energy. *J. Am. Chem. Soc.* **134**, 12104-12109 (2012).

- [52] Xiu, X., Puskar, N. L., Shanata, J. A. P., Lester, H. A. & Dougherty, D. A. Nicotine binding to brain receptors requires a strong cation- π interaction. *Nature* **458**, 534-537 (2009).
- [53] Hucher, M., Oberlin, A. & Hocart, R. Adsorption de vapeur d'eau sur les faces de clivage de quelques halogénures alcalins. *Bull. Soc. Fr. Mineral. Cristallogr.* **90**, 320-332 (1967).
- [54] Hu, J., Carpick, R. W., Salmeron, M. & Xiao, X. D. Imaging and manipulation of nanometer-size liquid droplets by scanning polarization force microscopy. *J. Vac. Sci. Technol. B* **14**, 1341-1343 (1996).
- [55] Phillips, J. C. et al. Scalable Molecular Dynamics with NAMD. *J. Comput. Chem.* **26**, 1781-1802 (2005).
- [56] MacKerell, A. D. et al. All-Atom Empirical Potential for Molecular Modeling and Dynamics Studies of Proteins. *J. Phys. Chem. B* **102**, 3586-3616 (1998).

ACKNOWLEDGMENT

We thank Drs. Yi Zhang, Jiang Li, Jingye Li, Qing Ji and Jijun Zhao for their constructive suggestions. This work was supported by the National Science Foundation of China (No. 11290164, 11404361 and 11204341), the Shanghai Natural Science Foundation of China under grant No. 13ZR1447900, the Knowledge Innovation Program of SINAP, the Supercomputer Center of Chinese Academy of Sciences and the Shanghai Supercomputer Center of China.

Author contributions.

G.S. and J.L. performed molecular dynamics simulations. H.F. and G.S. carried out most of the theoretical analysis. Y.S. and J.H. designed and observed the experimental investigation. C.W. and B.S. carried out some theoretical analysis. Y.W. carried out some experimental analysis. H.F., J.H. and G.S. contributed most of the ideas and wrote the paper. All authors discussed the results and commented on the manuscript.

Additional information

Supplementary information accompanies this paper on <http://www.nature.com/scientificreports>.

Competing financial interests: The authors declare that they have no competing financial interests.